Supporting information

Experimental Trends and Theoretical Descriptors for Electrochemical Reduction of Carbon Dioxide to Formate over Sn-based Bimetallic Catalysts

Xue Han, ‡[a] Binhong Wu, ‡[b] Yan Wang, ‡[c] Nathaniel N. Nichols[d], Yongjun Kwon[b], Yong Yuan[a], Zhenhua Xie[d], Sinwoo Kang[a], Byeongjun Gil[a], Caiqi Wang[b], Tianyou Mou[a], Hongfei Lin[b], Yao Nian*[e], Qiaowan Chang,*[b]

[a] Brookhaven National Laboratory, Upton, New York 11973, United States

[b] The Gene and Linda Voiland School of Chemical Engineering and Bioengineering, Washington State University, Pullman, WA 99164, United States

[c] School of Chemical Engineering, Sichuan University, Chengdu, 610065, PR China

[d] Department of Chemical Engineering, Columbia University, 500 W. 120th St., New York, NY 10027, United States

[e] School of Chemical Engineering and Technology, Tianjin University, Tianjin 300072, PR China

‡Xue Han, Binhong Wu and Yan Wang contributed equally to this work.

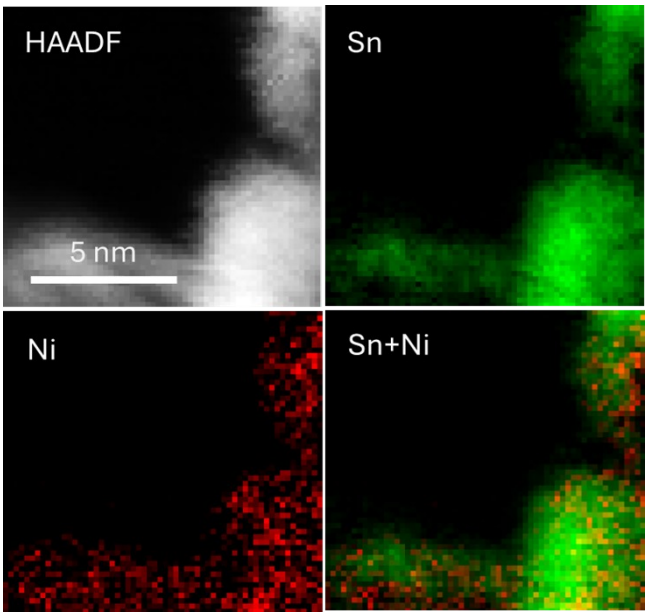

Figure S1. Scanning transmission electron microscopy and elemental mapping analysis of SnNi.

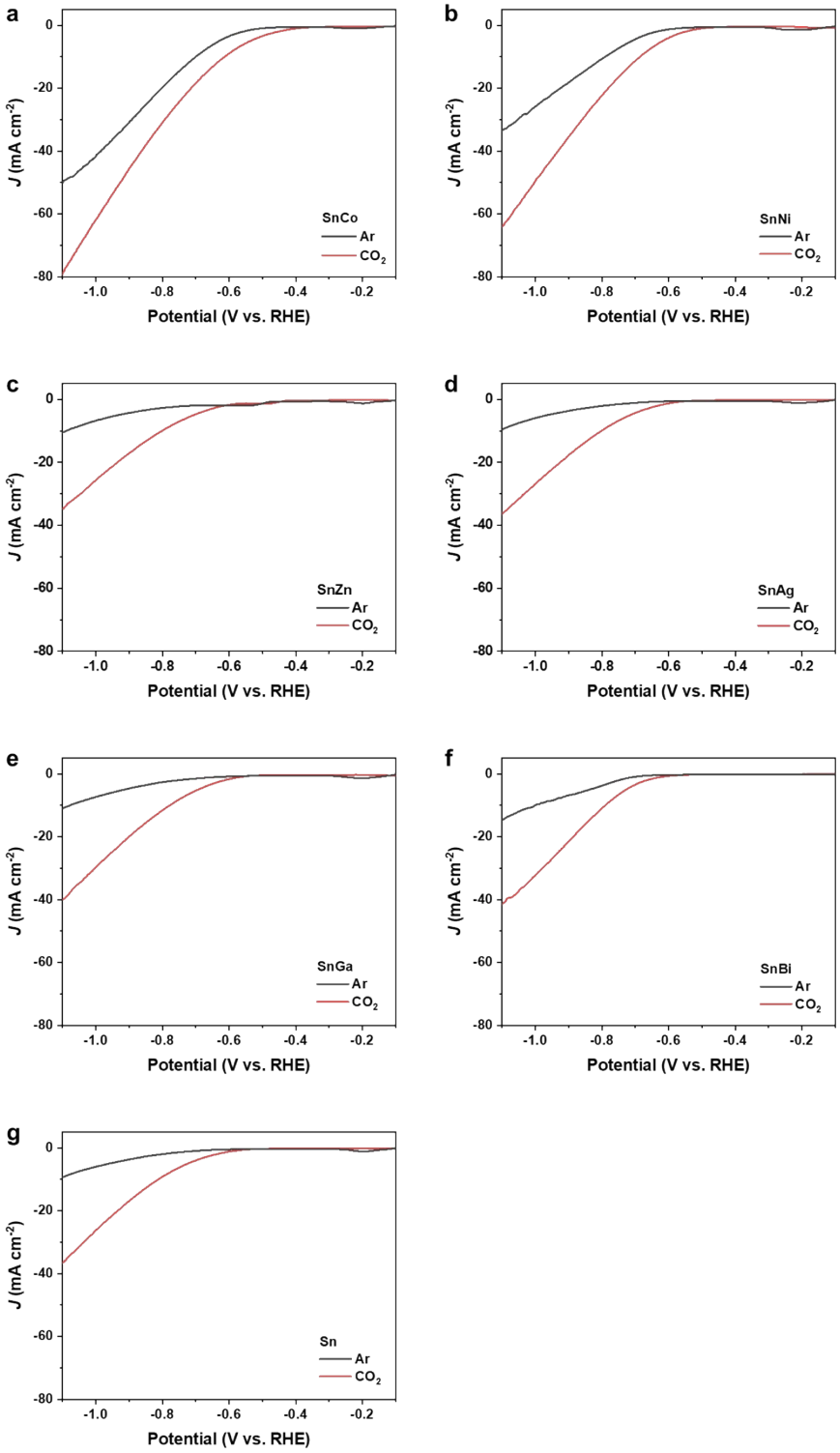

Figure S2. LSV curves of **a** SnCo, **b** SnNi, **c** SnZn, **d** SnAg, **e** SnGa, **f** SnBi and **g** Sn nanoparticles in Ar-saturated 0.5 M $KHCO_3$ electrolyte and CO_2-saturated electrolyte.

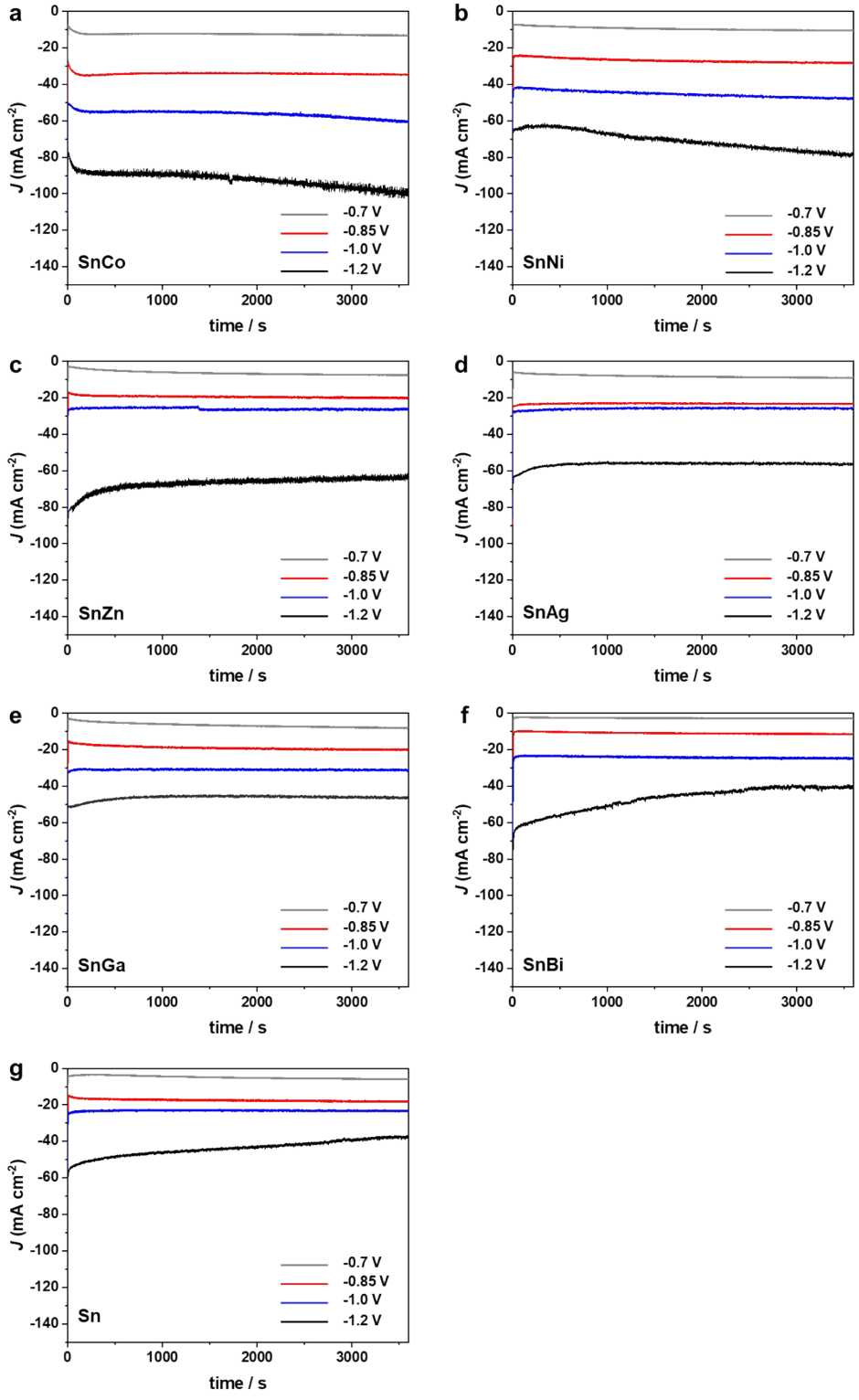

Figure S3. Chronoamperometric curves of **a** SnCo, **b** SnNi, **c** SnZn, **d** SnAg, **e** SnGa, **f** SnBi and **g** Sn at different potentials (vs. RHE).

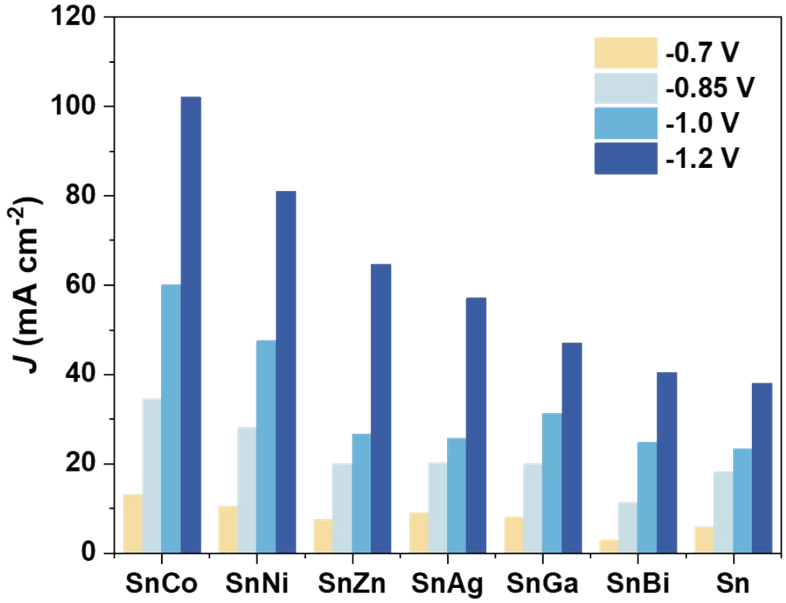

Figure S4. Total current density of SnCo, SnNi, SnZn, SnAg, SnGa, SnBi and Sn at different potentials (vs. RHE).

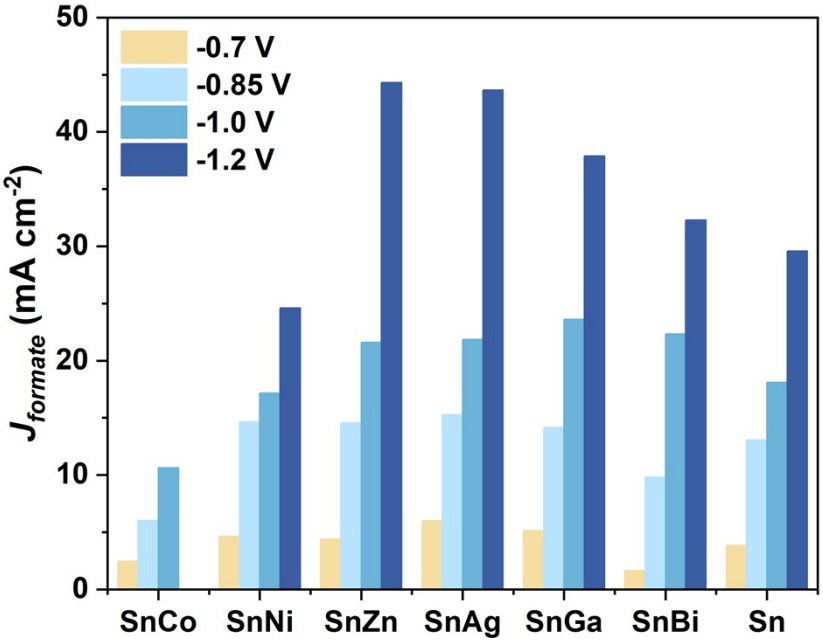

Figure S5. Partial current density of formate of SnCo, SnNi, SnZn, SnAg, SnGa, SnBi and Sn at different potentials (vs. RHE).

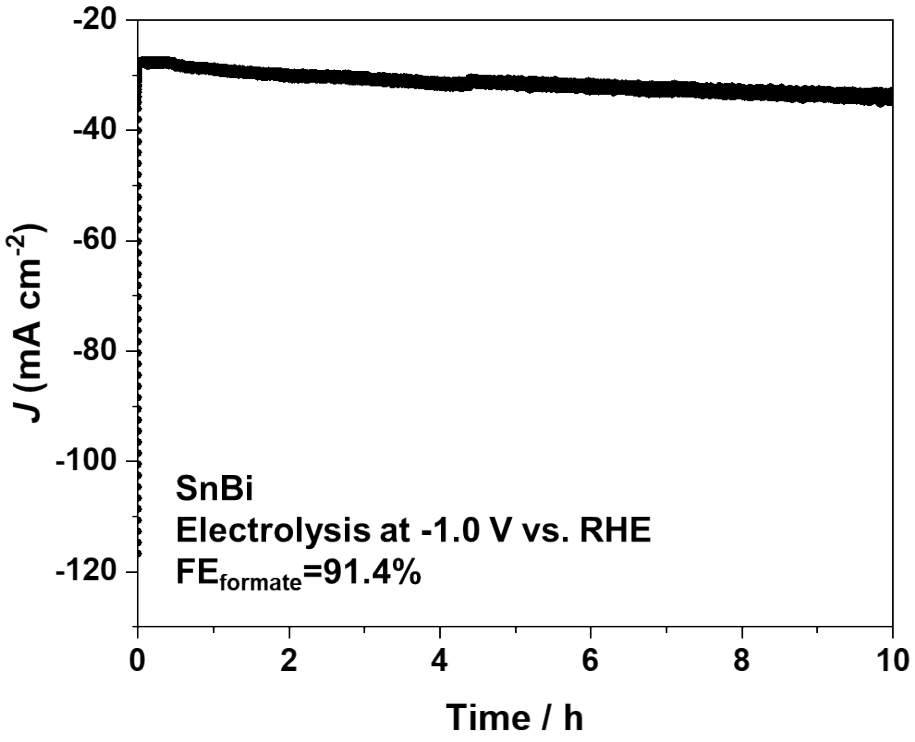

Figure S6. Stability test of SnBi for 10 h at -1.0 V.

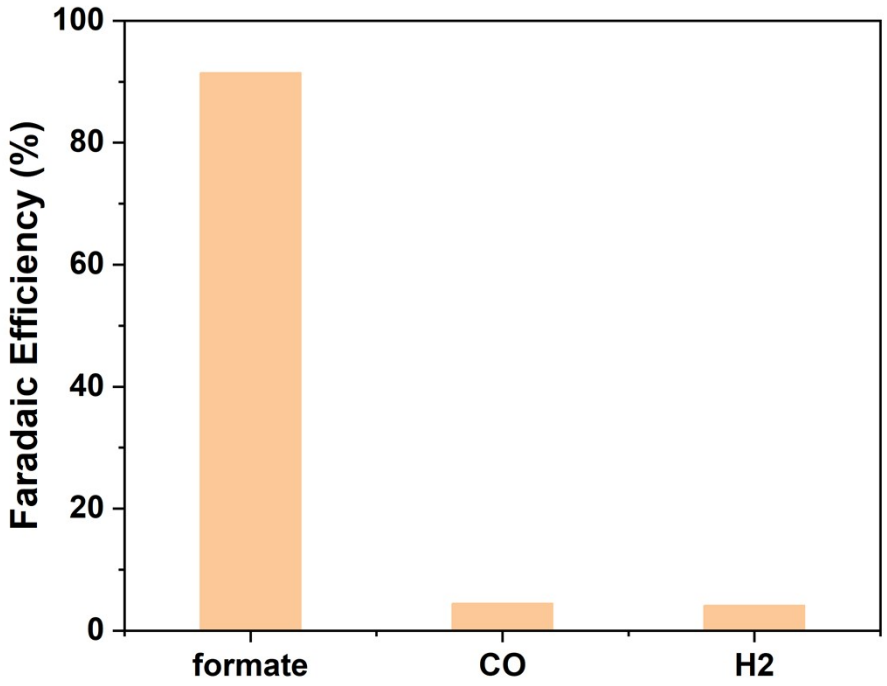

Figure S7. Faradaic efficiency of SnBi after 10 h.

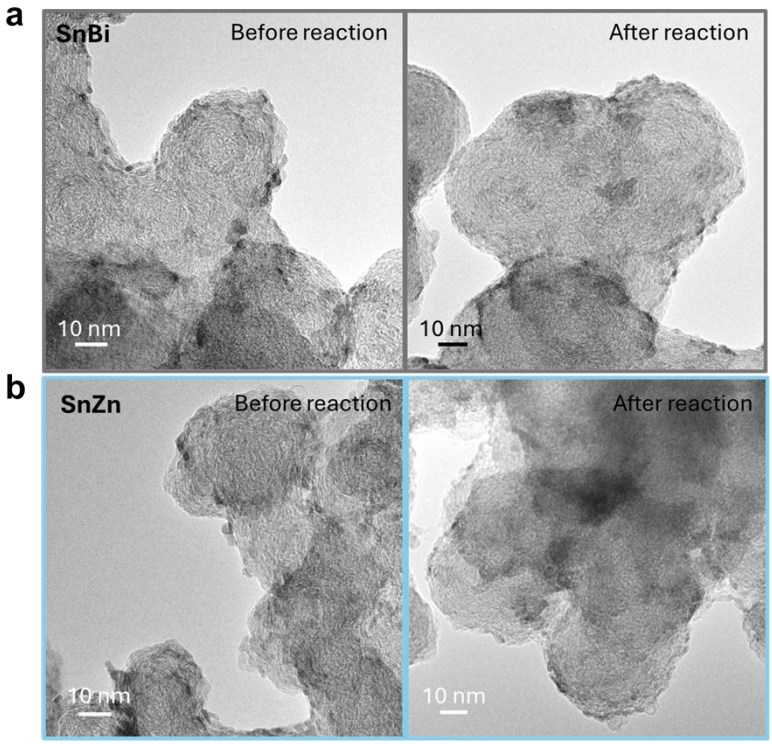

Figure S8. TEM images of SnBi and SnZn before and after the reaction.

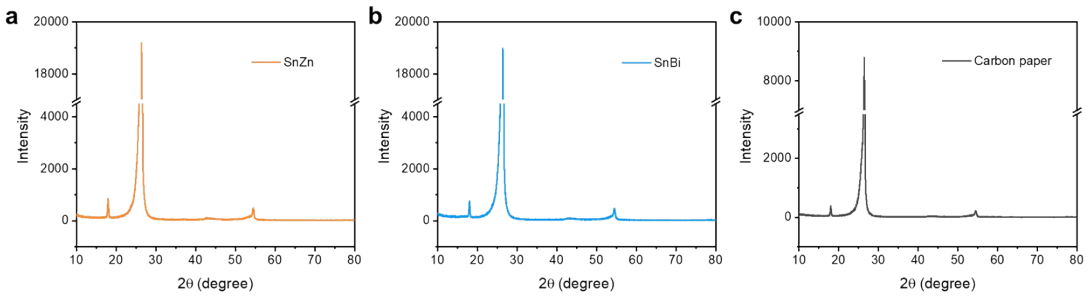

Figure S9. XRD patterns of SnBi and SnZn after the reaction.

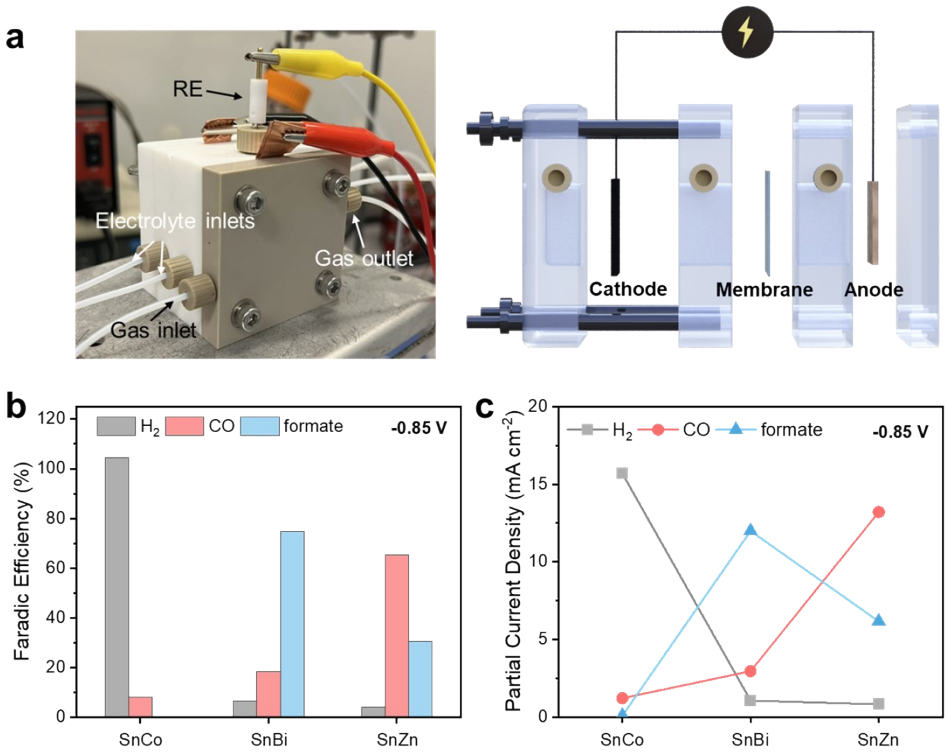

Figure S10. Flow cell test of SnCo, SnBi and SnZn. **a** schematic illustration of the flow cell experimental set-up, **b** FEs and **c** partial current densities of formate, CO, and H_2 at -0.85 V.

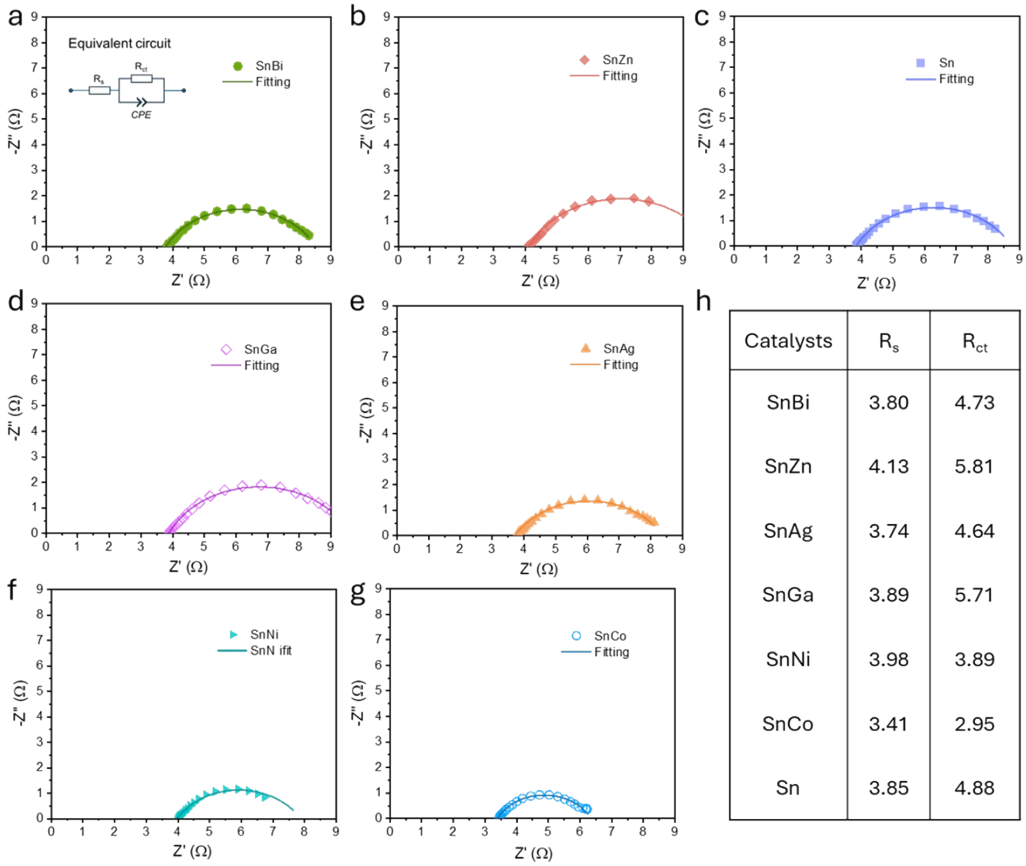

h

Catalysts	R_s	R_{ct}
SnBi	3.80	4.73
SnZn	4.13	5.81
SnAg	3.74	4.64
SnGa	3.89	5.71
SnNi	3.98	3.89
SnCo	3.41	2.95
Sn	3.85	4.88

Figure S11. EIS measurements of Sn-M catalysts at -0.9 V during CO_2RR. **a** SnBi, **b** SnZn, **c** Sn, **d** SnGa, **e** SnAg, **f** SnNi, **g** SnCo. **h** Fitting parameters obtained from Nyquist plots.

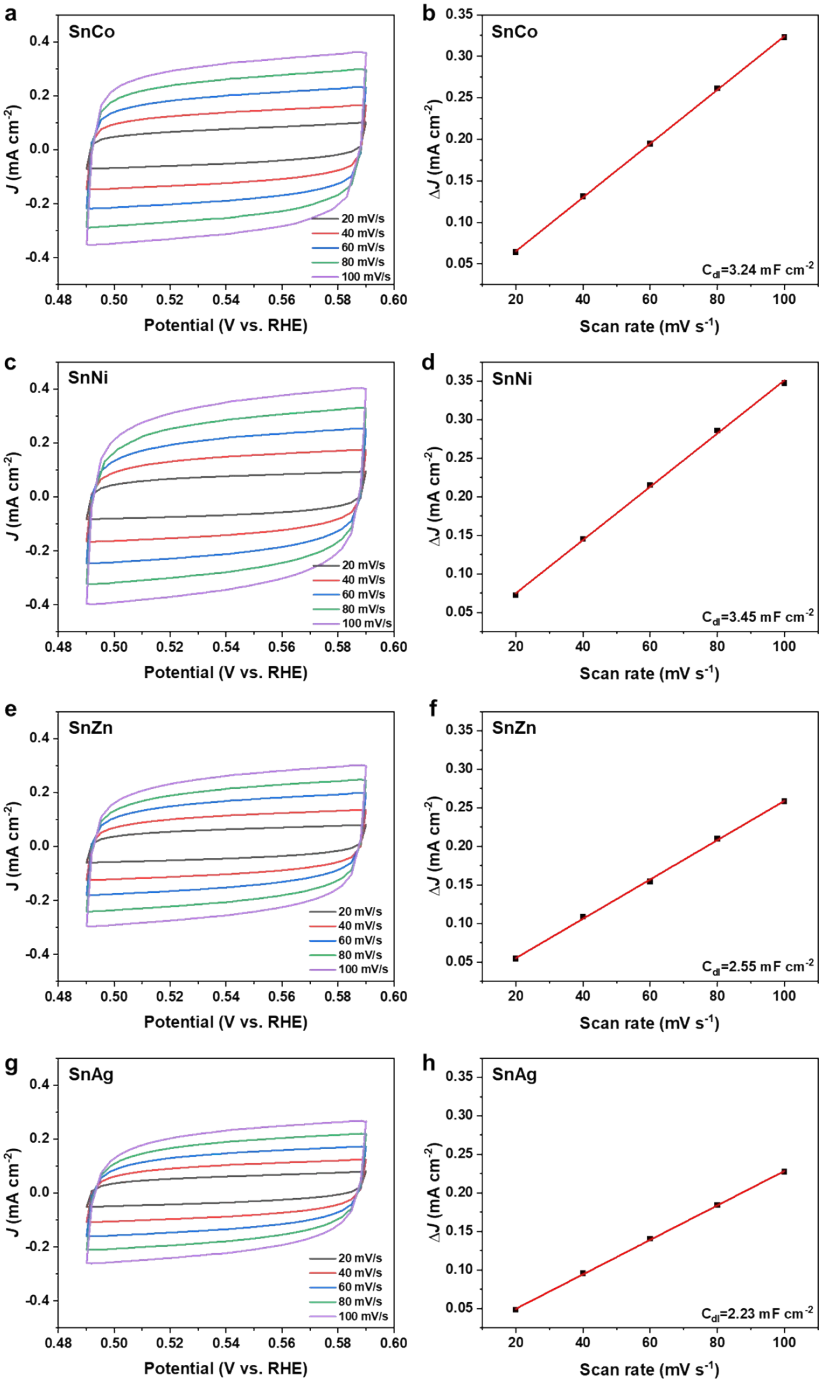

Figure S12. CV curves and corresponding C_{dl} for **a, b** SnCo, **c**, d SnNi, **e, f** SnZn and **g, h** SnAg, respectively.

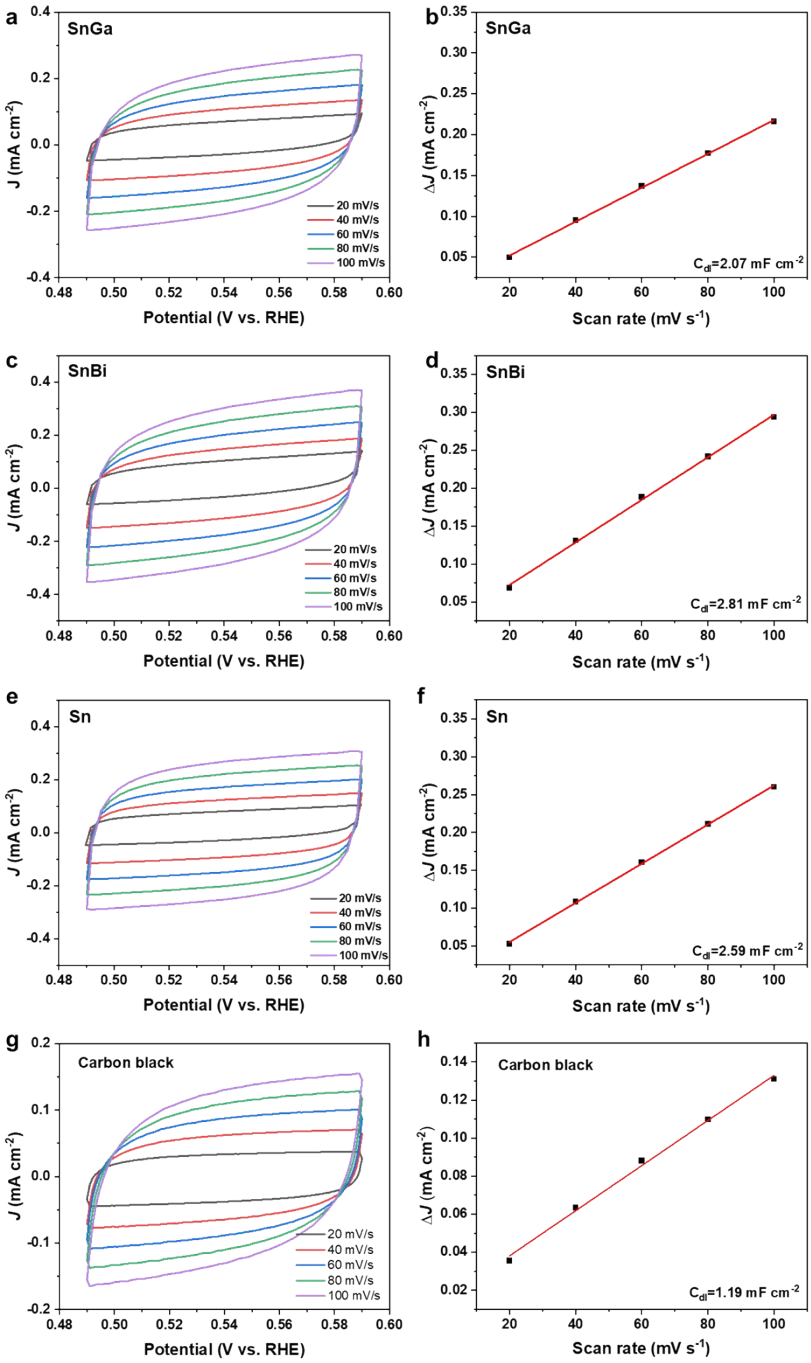

Figure S13. CV curves and corresponding C_{dl} for **a, b** SnGa, **c, d** SnBi, **e, f** Sn, and **g, h** carbon black, respectively.

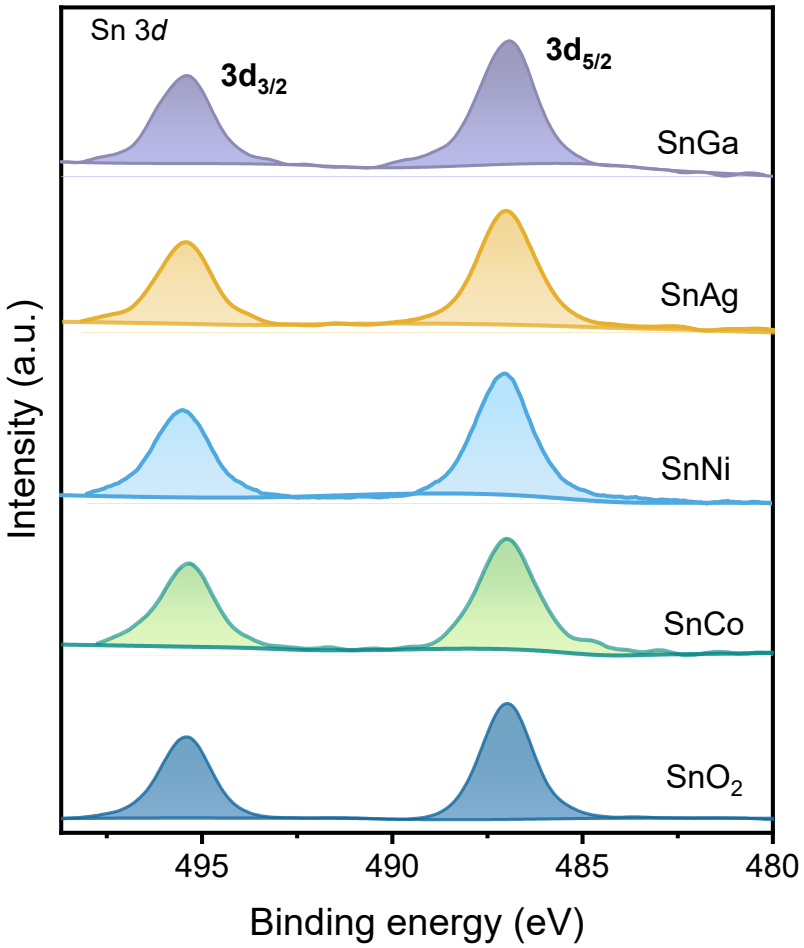

Figure S14. XPS Sn 3*d* spectra of SnGa, SnAg, SnNi, SnCo, and SnO_2 reference.

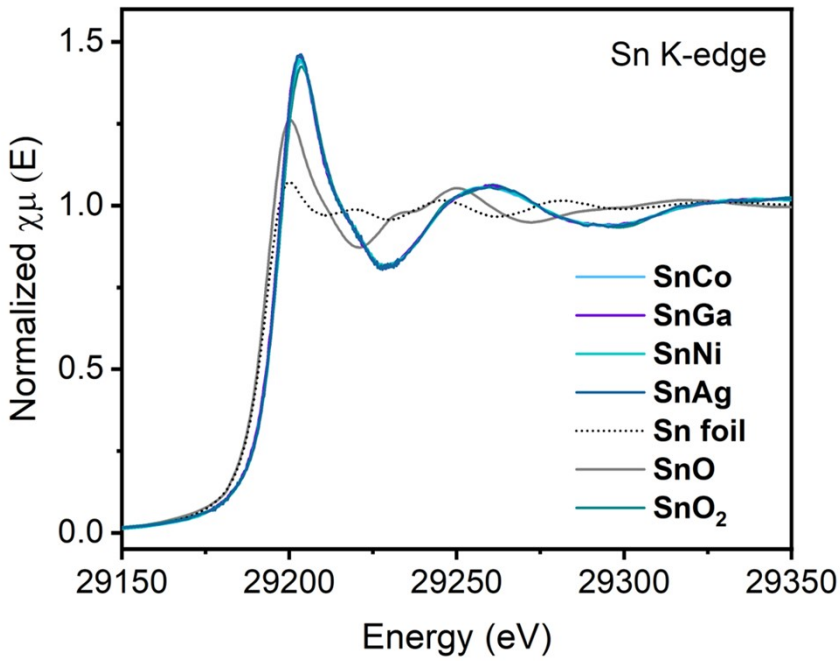

Figure S15. XANES spectra at the Sn K-edge of SnCo, SnGa, SnNi, SnAg, Sn foil, SnO, and SnO_2 standards.

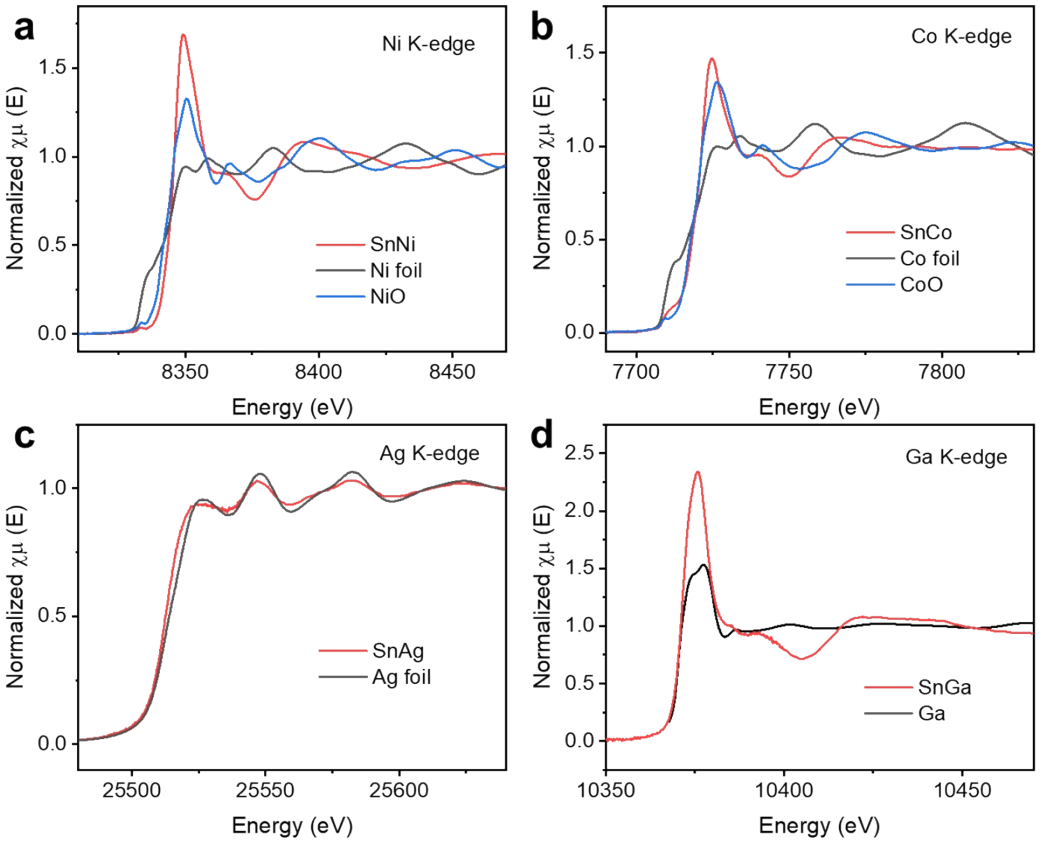

Figure S16. XANES spectra at the **a** Ni K-edge of SnNi, **b** Co K-edge of SnCo, **c** Ag K-edge of SnAg, **d** Ga K-edge of SnGa.

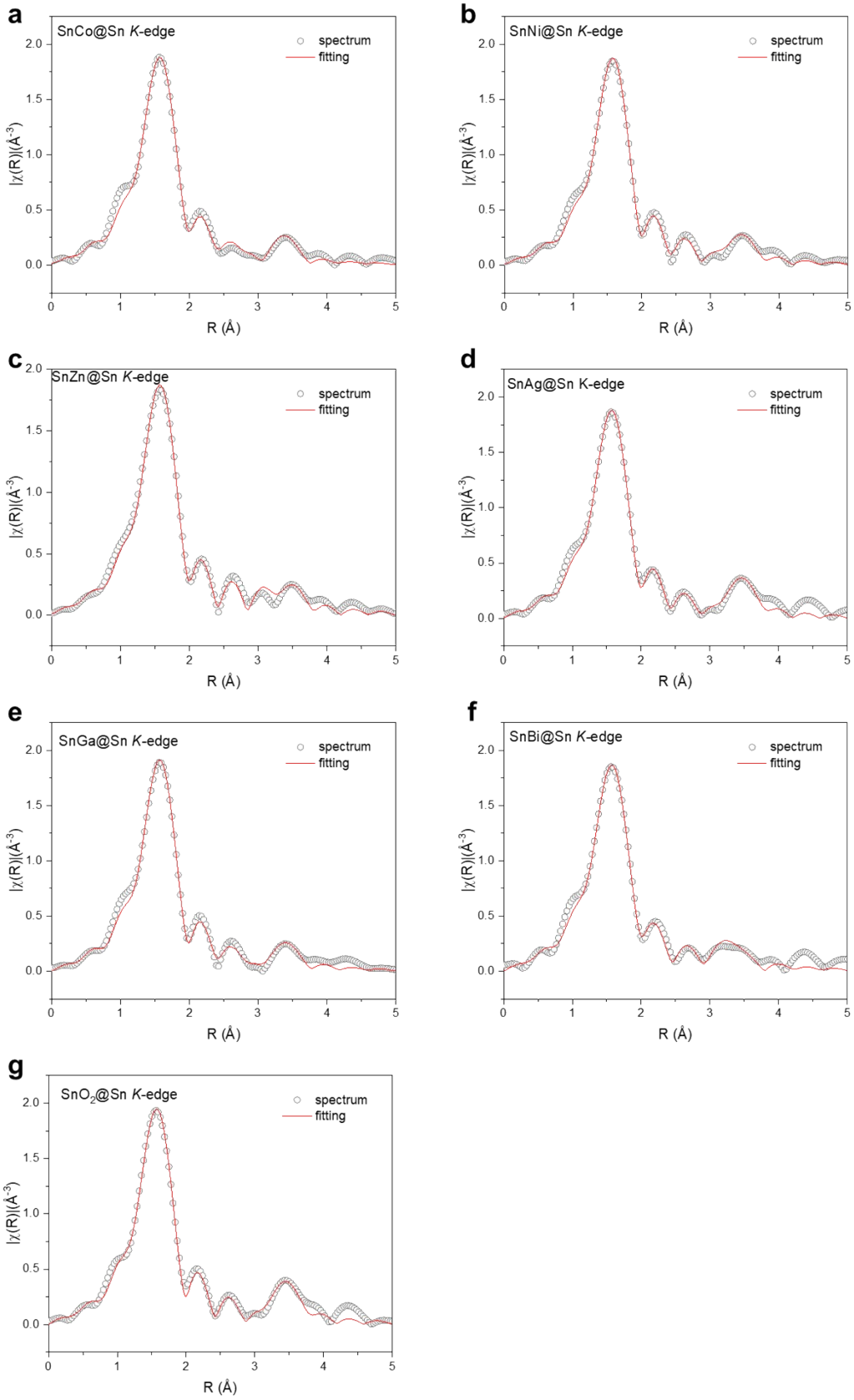

Figure S17. EXAFS fitting results of Sn-M bimetallic catalysts at Sn K-edge.

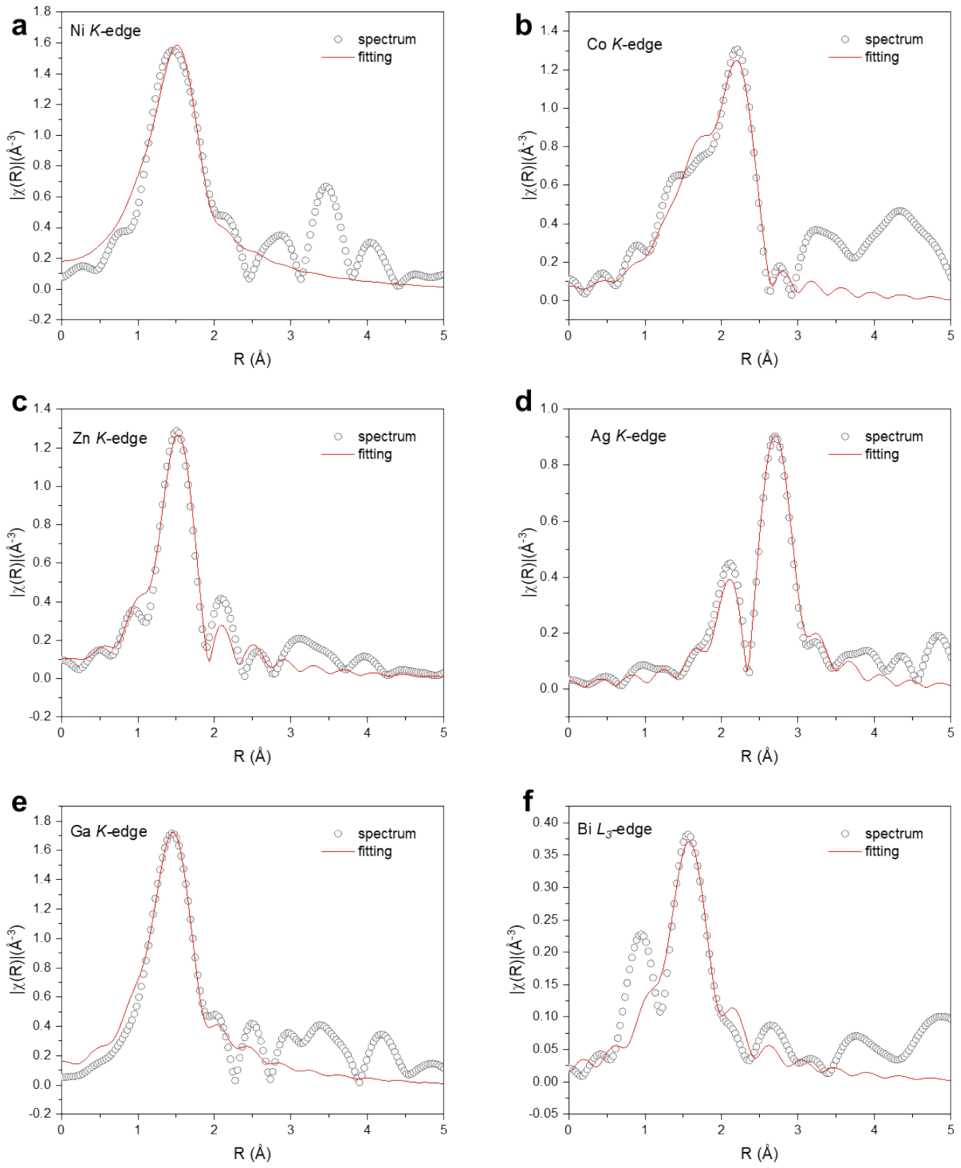

Figure 18. EXAFS fitting results of Sn-M bimetallic catalysts at Ni K-edge, Co K-edge, Zn K-edge, Ag K-edge, Ga K-edge, Bi L_3-edge.

Table S1. Fitting results of the Sn K-edge FT-EXAFS spectra over the SnM samples.

Samples	Shell	CN	Bond length (Å)	σ^2 (Å^2)	E_0 shift (eV)	R factor
SnO_2	Sn-O	6.0 ± 0.4	2.05 ± 0.01	0.0033	7.6	0.011
	Sn-O-Sn^a	1.3 ± 0.4	3.23 ± 0.02			
	Sn-O-Sn^b	2.5 ± 0.7	3.73 ± 0.02			
SnZn	Sn-O	6.1 ± 0.3	2.05 ± 0.01	0.0040	8.1	0.007
	Sn-O-Sn^a	1.2 ± 0.3	3.21 ± 0.02			
	Sn-O-Sn^b	1.6 ± 0.5	3.74 ± 0.02			
SnGa	Sn-O	5.8 ± 0.4	2.05 ± 0.01	0.0032	7.6	0.009
	Sn-O-Sn^a	0.8 ± 0.4	3.24 ± 0.03			
	Sn-O-Sn^b	1.3 ± 0.6	3.72 ± 0.03			
SnBi	Sn-O	6.5 ± 0.3	2.06 ± 0.01	0.0046	7.8	0.006
	Sn-O-Sn^a	1.7 ± 0.3	3.24 ± 0.01			
	Sn-O-Sn^b	1.3 ± 0.5	3.73 ± 0.03			
SnNi	Sn-O	5.9 ± 0.3	2.05 ± 0.01	0.0064	8.1	0.004
	Sn-O-Sn^a	0.9 ± 0.3	3.23 ± 0.02			
	Sn-O-Sn^b	1.7 ± 0.5	3.73 ± 0.02			
SnCo	Sn-O	6.1 ± 0.3	2.05 ± 0.00	0.0041	8.0	0.005
	Sn-O-Sn^a	0.8 ± 0.3	3.25 ± 0.02			
	Sn-O-Sn^b	1.4 ± 0.4	3.71 ± 0.02			
SnAg	Sn-O	6.1 ± 0.4	2.05 ± 0.01	0.0039	7.7	0.008
	Sn-O-Sn^a	1.2 ± 0.4	3.24 ± 0.02			
	Sn-O-Sn^b	2.5 ± 0.6	3.74 ± 0.02			

Notes: CN—average coordination number (normalized to all the absorbers) around the absorbing center atom; σ^2—mean square variation in path length; R-factor—quality of fitting. The "a" and "b" represented the shorter and longer Sn-O-Sn bonds, respectively. Fitting ranges: $3.0 < k < 11$ Å^{-1}, $1 < R < 4$ Å; $k^1k^2k^3$-weighted multiple EXAFS fittings.

Table S2. Fitting results of the Zn K-edge, Ga K-edge, Bi L_3-edge, Ni K-edge, Co K-edge, and Ag K-edge FT-EXAFS spectra over the SnM samples.

Samples	Shell	CN	Bond length (Å)	σ^2 ($Å^2$)	E_0 shift (eV)	R factor
SnZn Zn K-edge	Zn-O	3.2 ± 0.5	1.97 ± 0.01	0.0015	-0.9	0.030
SnGa Ga K-edge	Ga-O	6.7 ± 1.0	1.92 ± 0.02	0.0073	0.4	0.023
SnBi Bi L_3 K-edge	Bi-O[a]	2.3 ± 1.1	2.16 ± 0.04	0.0046	-4.0	0.065
	Bi-O[b]	1.2 ± 0.5	2.36 ± 0.08			
SnNi Ni K-edge	Ni-O	9.9 ± 1.9	2.01 ± 0.03	0.0130	-5.6	0.022
SnCo Co K-edge	Co-O	3.8 ± 0.7	2.08 ± 0.01	0.0064	-0.1	0.021
	Co-Co	3.7 ± 0.9	2.50 ± 0.01	0.0064	-0.1	0.021
SnAg Ag K-edge	Ag-Ag	7.6 ± 0.8	2.87 ± 0.01	0.0104	0.6	0.019

Notes: CN—average coordination number (normalized to all the absorbers) around the absorbing center atom; σ^2—mean square variation in path length; R-factor—quality of fitting. The "a" and "b" represented the shorter and longer Bi-O bonds, respectively. Fitting ranges: 3.0 < k < 11 (or 10.5) $Å^{-1}$, 1 (or 1.1) < R < 3 (or 3.3) Å; $k^1k^2k^3$-weighted multiple EXAFS fittings.

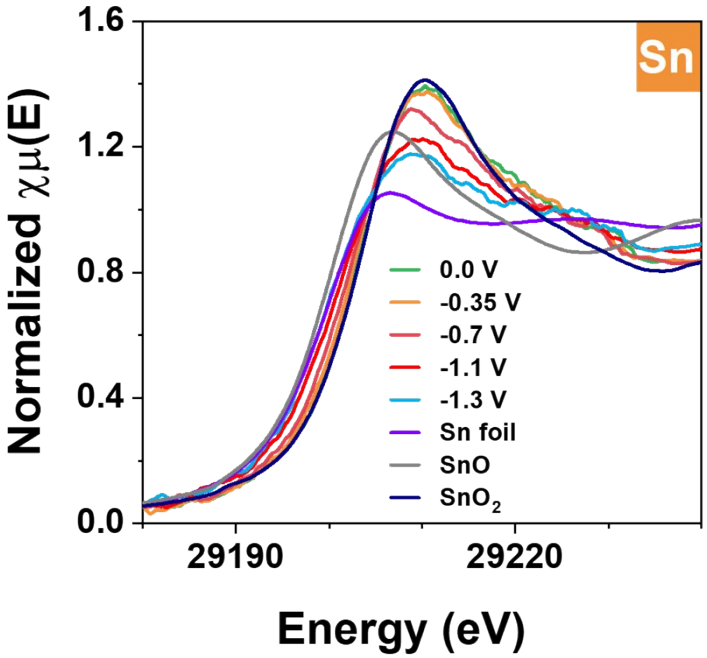

Figure S19. The *in-situ* Sn K-edge XANES spectra over Sn/C catalysts under different potentials.

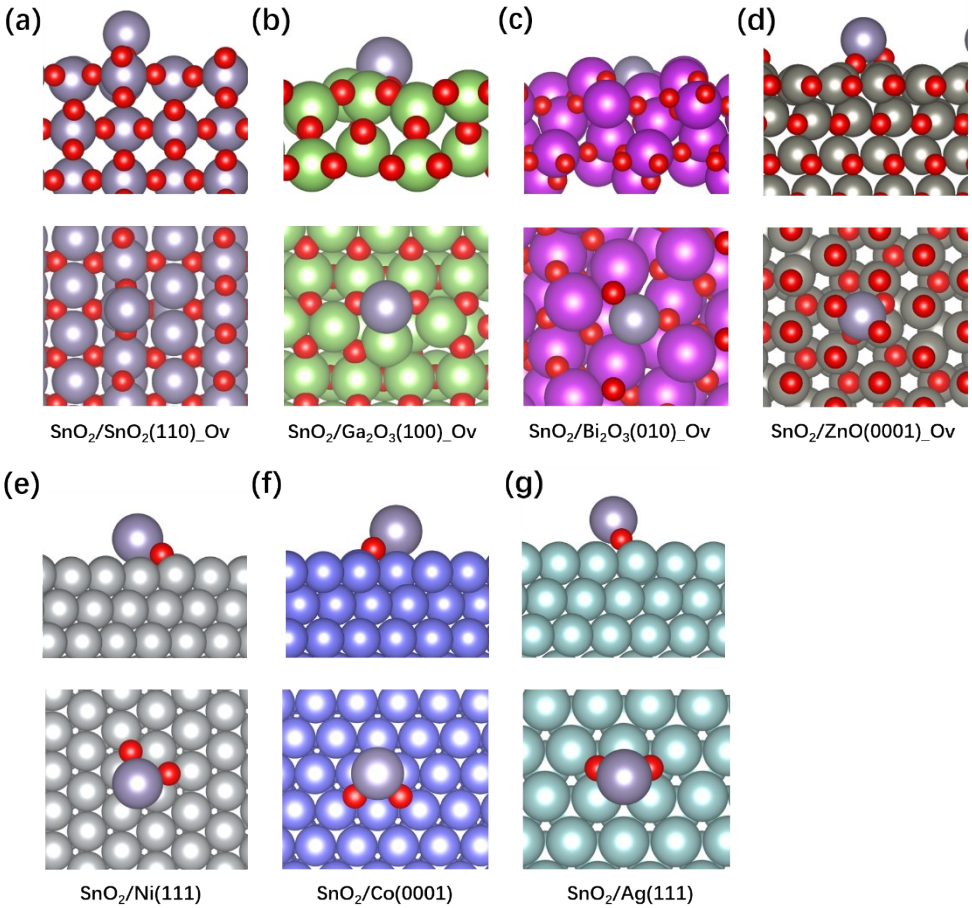

Figure S20. Top and side view of DFT optimized configurations of **a** $SnO_2/SnO_2(110)\_O_v$, **b** $SnO_2/Ga_2O_3(100)\_O_v$, **c** $SnO_2/Bi_2O_3(010)\_O_v$, **d** $SnO_2/ZnO(0001)\_O_v$, **e** $SnO_2/Ni(111)$, **f** $SnO_2/Co(0001)$ and **g** $SnO_2/Ag(111)$. Red, gray purple, green, pink, dark gray, light gray, purple and cyan ball are represent O, Sn, Ga, Bi, Zn, Ni, Co and Ag atoms, respectively.

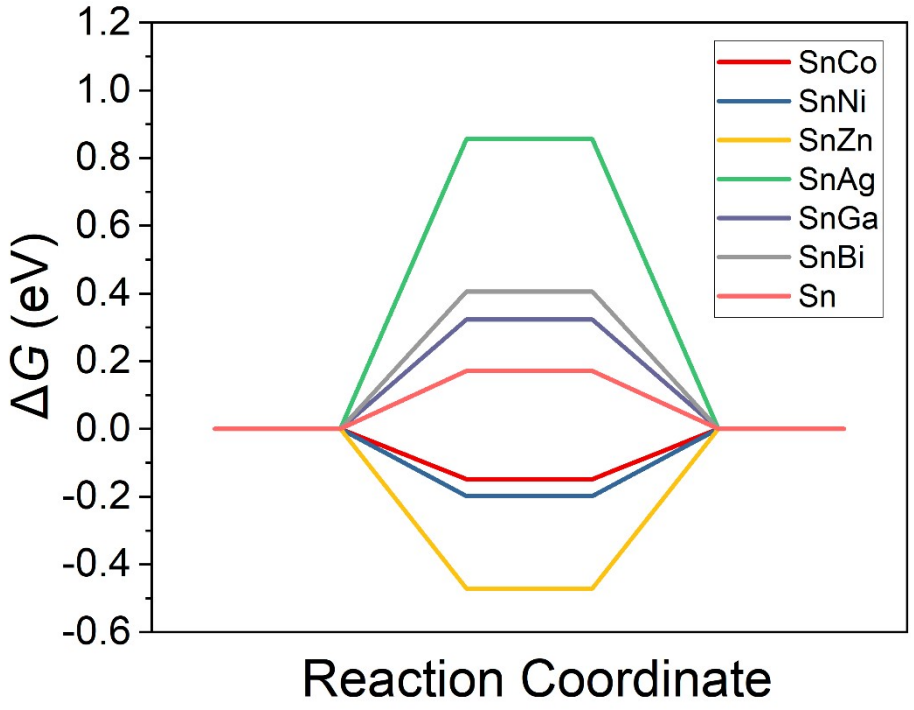

Figure S21. The free energy diagrams of HER on Sn-based catalysts.

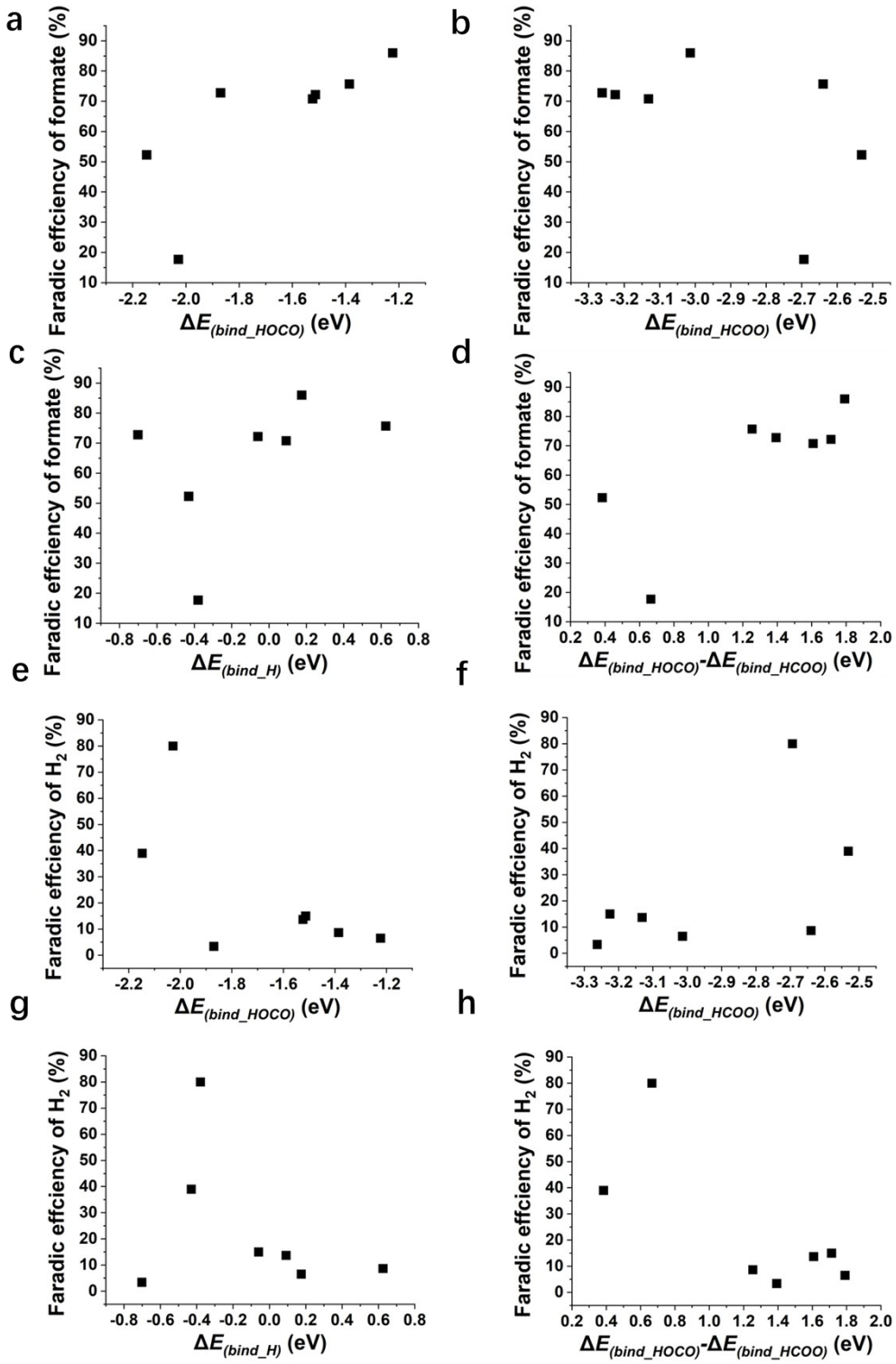

Figure S22. Correlation of **a** $\Delta E_{(\text{bind\_HOCO})}$, **b** $\Delta E_{(\text{bind\_HCOO})}$, **c** $\Delta E_{(\text{bind\_H})}$, and **d** $\Delta E_{(\text{bind\_HOCO})}$-$\Delta E_{(\text{bind\_HCOO})}$ versus $\text{FE}_{\text{formate}}$ at −0.85 V vs. RHE. Correlation of **e** $\Delta E_{(\text{bind\_HOCO})}$, **f** $\Delta E_{(\text{bind\_HCOO})}$, **g** $\Delta E_{(\text{bind\_H})}$, and **h** $\Delta E_{(\text{bind\_HOCO})}$-$\Delta E_{(\text{bind\_HCOO})}$ versus FE_{H2} at −0.85 V vs. RHE.

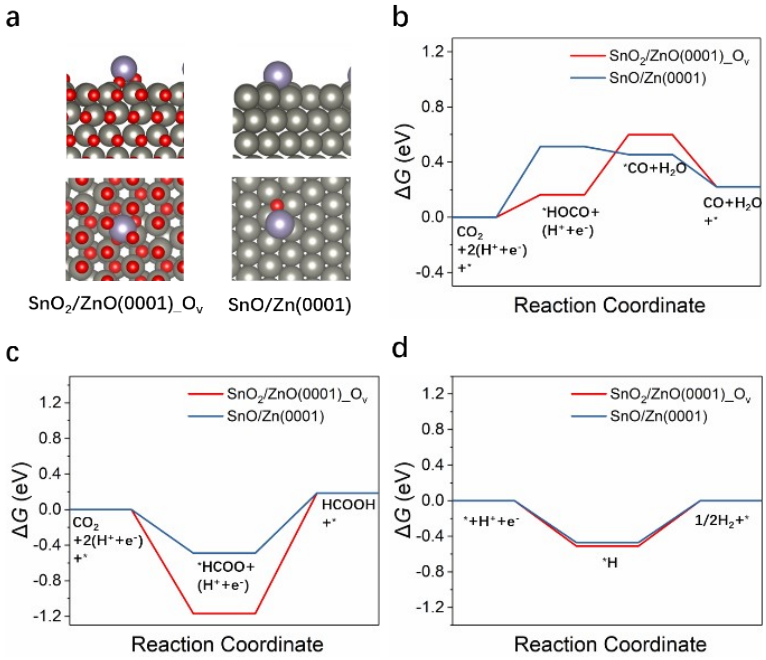

Figure S23. **a** Top and side view of DFT optimized configurations of SnO_2/ZnO(0001)_O_v and SnO/Zn(0001). The free energy diagrams of CO_2 conversion to **b** CO, **c** HCOOH and **d** H_2.